HiL pantograph tests with a realistic catenary model including overlap section

Manuel Tur[a], Santiago Gregori[a,*], Stefano Bruni[b], Alan Facchinetti[b]

[a] *Instituto de Ingeniería Mecánica y Biomecánica, Universitat Politècnica de València, València, Spain*
[b] *Dipartimento di Meccanica, Politecnico di Milano, Milano, Italy*

Abstract

For pantograph-catenary systems, Hardware-in-the-Loop (HiL) testing represents a valuable tool to partly replace expensive and logistically complex in-line tests. However, the regulatory acceptance of such methodologies requires excellent accuracy while keeping real-time performance. This paper proposes a methodology to perform HiL pantograph tests utilizing a high-fidelity finite element catenary model that incorporates overlap sections and the simultaneous interaction of a pantograph with two contact wires through a penalty-based formulation. Without loss of generality, the Italian C270 overhead line and the ATR 95 pantograph have been chosen to exemplify the proposed method.

To achieve the real-time execution required for HiL environments, the conventional PACDIN software algorithm was modified introducing five simplifying hypotheses. These actions successfully reduced the computational cost while maintaining a high accuracy. System stability and force tracking were ensured using an interaction mass and an LQG controller, mitigating the effect of delays and actuator dynamics. The proposed methodology was validated in a two-stage process: first, by demonstrating good agreement between the real-time algorithm and conventional solvers, then, by comparing HiL results with experimental measurements obtained from an instrumented pantograph during in-line tests. The results show a relative difference in the contact force standard deviation of only 6.2 %, falling within the acceptable limits defined by the EN 50318 standard. This work represents a significant milestone in developing robust HiL tools capable of simulating complex overhead contact line discrete features with the accuracy required for high-speed railway applications.

Keywords: Hardware-in-the-Loop, LQG control, Actuator dynamics, C270 catenary, Overlap section

1. Introduction

1.1. Background

The dynamic interaction between the pantograph and the overhead contact line (OCL) is a determining factor for ensuring efficient and safe energy collection in electrified railway transport [1]. Currently, the commissioning and certification processes for

*Corresponding author
Email address: sangreve@upv.es (Santiago Gregori)

new lines and rolling stock are strictly regulated by international standards, such as EN 50317 [2] and EN 50367 [3]. These regulations mandate extensive experimental track tests to assess current collection quality. However, field tests are remarkably expensive, logistically complex, and dependent on limited time windows within commercial railway operations. Consequently, there is a growing interest in Hardware-in-the-Loop (HiL) testing, also known as hybrid simulation (HS). This methodology has the potential to replace, at least partially, expensive in-line measurements, provided that the reliability and precision of the laboratory results are high enough to meet the stringent safety and performance requirements of regulatory bodies.

1.2. Catenary description and research problem

A high-speed catenary is a complex overhead infrastructure designed to provide uninterrupted electrical power supply to trains through sliding contact with the pantograph. Structurally, it consists of several key components engineered to maintain as uniform contact wire height and elasticity as possible. The primary elements include the contact wire, the messenger wire (or catenary wire), and the droppers connecting the contact and messenger wires. In high-speed systems, such as the Italian C270 catenary studied in this work, the precise tensioning and installation of these components are critical to produce a stable and safe current collection.

Current research is focused on the need for accurate catenary models to conduct reliable Hardware-in-the-Loop (HiL) tests. However, there is an inherent technical contradiction: the more realistic and detailed a model becomes (e.g., using high-fidelity Finite Element formulations), the higher its computational cost. This calculation burden is usually incompatible with the real-time execution in a HiL test bench. Therefore, the focus of this article is to resolve this technical compromise, enabling the execution of HiL tests with high-fidelity catenary models solved in real-time.

1.3. State of the art

Hardware-in-the-Loop (HiL) testing represents a well-established approach in some fields of the railway engineering, bridging the gap between high-fidelity numerical models and costly field measurements. As noted in [4], the concept of HiL for pantograph-catenary interaction dates back to 2002, initially utilizing hydraulic actuators and simplified modal catenary models [5, 6]. Since then, various research groups have advanced the technology by incorporating different actuation principles, such as electrohydraulic [7] or electric [8] drives, and more sophisticated virtual environments. However, HiL testing for pantographs is currently an open research topic and has not yet reached acceptance from the railway industry.

A central challenge highlighted in the literature is the real-time requirement for the virtual catenary. Due to these strict timing constraints, catenary models in HiL tests have historically relied on significant simplifications that limit their accuracy. Early implementations utilized a modal basis with a limited number of spans [9, 10] or infinite tensioned strings supported by viscoelastic layers [11]. More advanced strategies include the use of pantograph-fixed coordinates [12] or periodic finite element formulations [13]. While these models capture the fundamental wave propagation phenomena, they often fail to represent the geometric singularities found in the real infrastructure.

Recent research has focused on overcoming these limitations by integrating general Finite Element (FE) models of entire tension lengths into the real-time loop [14]. To

ensure the stability of these advanced HS setups, researchers have implemented various control strategies, ranging from impedance control via Model Predictive Control (MPC) [15] to Linear-Quadratic Gaussian (LQG) [14] controllers. Furthermore, methodologies such as the dynamically substructured system framework [16] have been proposed to mitigate instabilities caused by communication delays or modeling errors.

Despite these advancements, the reliable simulation of discrete features, such as overlap sections, within a real-time HiL environment remains a challenging milestone. While some recent methodologies [17] allow for the use of complex catenary models through iterative, non-real-time coupling, the achievement of a truly robust, real-time HiL test that maintains the high precision required for certification purposes is still a primary research objective. The present work contributes to this effort by proposing a real-time FE methodology capable of handling these complex geometric features without compromising the accuracy required for high-speed applications.

1.4. Contributions

This paper proposes a comprehensive methodology to perform HiL tests using a realistic FE catenary model that includes overlap sections. As a case study, a high-fidelity model of the Italian C270 catenary is developed, implementing an overlap section where the ATR 95 pantograph interacts with two contact wires using a penalty-based contact method. Starting from the conventional algorithm used in the PACDIN software [18], different simplifying hypotheses are introduced to achieve real-time execution without significantly compromising accuracy. To ensure stability and precise force tracking in the HiL tests, and to compensate for the delays inherent to the HiL testing procedure, the implementation of an LQG controller is proposed. Additionally, specific actions are proposed for the development of HiL tests in the overlap section, such as the use of an interaction mass and the distribution of the measured force over multiple contact wires. Finally, the real-time algorithm is validated by comparison with conventional solvers, and the HiL test results are validated against experimental measurements obtained in track tests.

1.5. Organization of the paper

After this introduction, Section 2 describes the finite element model of the C270 catenary and of the ATR 95 pantograph, and the simplifying assumptions introduced to achieve a real-time simulation from the conventional algorithm used in the PACDIN software. Section 3 details the HiL test rig setup and the LQG control strategy, while Section 4 presents the numerical results and validation of the proposed methodology. Finally, Section 5 summarizes the main conclusions and future work.

2. Models description

In this section, catenary and pantograph models used to perform pure numerical simulations of the pantograph-catenary dynamic interaction problem are first presented. Then, different simplifications applied to the catenary model to achieve real-time performance required in HiL tests are described.

2.1. Catenary model

The finite element method, with an absolute nodal coordinate formulation (ANCF) [19], is applied to model the two tension lengths of the Italian C270 catenary considered in this work (see Figure 1). Specifically, contact and messenger wires are modeled using beam elements while droppers and steady arms are considered as bar elements. Clamps between the different wires are accounted as point masses and appropriate boundary conditions are applied to both ends of each tension length and to the connection of the steady arms with the registration arms. The messenger wire supports are replaced by spring-damper elements. The geometric parameters and material properties of the catenary model are given in Appendix A.

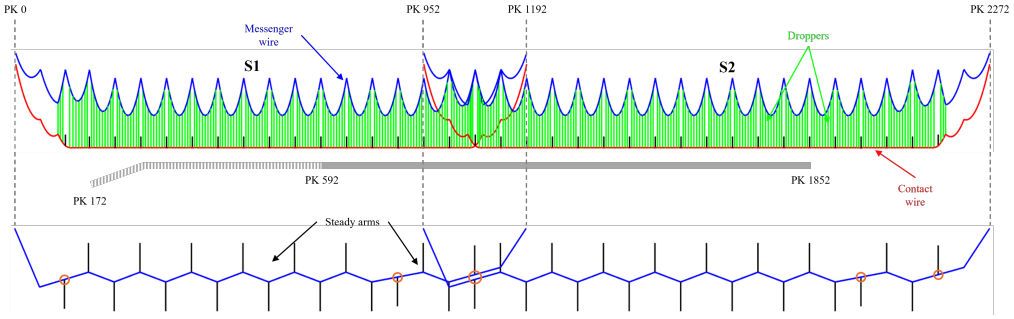


Figure 1: *Lateral (top image) and top (bottom image) views of the finite element model of two tension lengths, S1 and S2, of the Italian C270 catenary, corresponding to the section of the Torino-Milano line from km 54.485 to km 56.757.*

To obtain the initial configuration of the catenary model, a shape-finding problem is solved in which both the nodal coordinates $\mathbf{u_0}$ and the undeformed element lengths $\mathbf{l}$ are found to fulfill the static equilibrium of the catenary and, at the same time, some design constraints on the static configuration of the system. The equations describing the shape-finding problem are:

$$\begin{aligned} \mathbf{F}_{\mathrm{e}}(\mathbf{u_0}, \mathbf{l}) - \mathbf{F}_{\mathrm{g}}(\mathbf{l}) &= \mathbf{0} \\ \mathbf{C}(\mathbf{u_0}, \mathbf{l}) &= \mathbf{0} \end{aligned} \tag{1}$$

in which $\mathbf{F}_{\mathrm{e}}$ and $\mathbf{F}_{\mathrm{g}}$ are the global vectors of elastic and gravitational forces, respectively, and $\mathbf{C}$ is a set of equations to impose contact wire height at dropper connection points, messenger and contact wire mechanical tension, and the position of droppers, steady arms and messenger wire supports. This is a non-linear problem that can be solved by applying the Newton-Raphson method [20].

It is important to note that the contact wire height profile of an actual catenary after installation may differ from the nominal one due to installation, assembly or manufacturing errors. To include these irregularities of the contact wire height, after the nominal initial configuration is obtained, the undeformed length of the bar elements used to model the droppers can be changed accordingly, and then, the equilibrium equations (first equation in Eq. (1)) must be solved to compute the nodal coordinates of the new static configuration.

The catenary dynamic behavior under the action of the pantograph is governed by small displacements so that it can be linearised around the static configuration. This leads to:

$$\mathbf{M}_\mathrm{c}\ddot{\mathbf{u}}_\mathrm{c}^t + \mathbf{C}_\mathrm{c}\dot{\mathbf{u}}_\mathrm{c}^t + \mathbf{K}_\mathrm{c}\mathbf{u}_\mathrm{c}^t = {\mathbf{N}_\mathrm{c}^t}^\mathrm{T} F_\mathrm{c}^t + {\mathbf{N}_\mathrm{d}}^\mathrm{T}\mathbf{F}_\mathrm{d}^t \tag{2}$$

where $\mathbf{u}_\mathrm{c}^t$, $\dot{\mathbf{u}}_\mathrm{c}^t$, $\ddot{\mathbf{u}}_\mathrm{c}^t$ are the nodal displacements, velocities and accelerations at time $t \in [1, N_\mathrm{t}]$; $\mathbf{K}_\mathrm{c}$, $\mathbf{C}_\mathrm{c}$, $\mathbf{M}_\mathrm{c}$ are the stiffness, damping and mass matrices, F_c^t is the vertical contact force between the pantograph and catenary, $\mathbf{F}_\mathrm{d}^t$ is the vector containing the correction forces, defined as the magnitude of the compressive additional force applied to each dropper. For a given dropper j, this magnitude $\mathbf{F}_{\mathrm{d}j}^t$, is positive if dropper j is slackened and 0 otherwise. $\mathbf{N}_\mathrm{c}^t$ is the interpolation matrix that maps the generalised nodal coordinates of the FE model to the contact wire displacement at the contact point, while ${\mathbf{N}_\mathrm{d}}^\mathrm{T}$ maps $\mathbf{F}_\mathrm{d}^t$ to the generalised nodal forces of the two ends of each dropper in compressive direction. When more than one tension length is considered, as in this case, multiple sets of equations in the form of Eq. (2) are considered, one for each tension length.

Note that Eq. (2) is non-linear since both F_c^t and $\mathbf{F}_\mathrm{d}^t$ depend non-linearly on the displacements $\mathbf{u}_\mathrm{c}^t$ to consider pantograph contact losses (defined here as the mechanical separation between the collectors and the contact wire), and dropper slackening. Figure 2 shows the bilinear traction-elongation curve of a given dropper $j \in [1, N_\mathrm{dr}]$, being the stiffness of dropper j in compression λ times its stiffness in traction $k_{\mathrm{d}j}$. To find out if a given dropper j is tensioned, the following condition is checked:

$$\mathbf{F}_{\mathrm{d}j}^0 + \mathbf{K}_{\mathrm{dr}j}\mathbf{u}_\mathrm{c}^t \geq 0 \tag{3}$$

where $\mathbf{F}_\mathrm{d}^0$ is the vector that contains the force transmitted by each dropper in the static configuration. Note that using the sign convention defining $\mathbf{N}_\mathrm{d}$, $\mathbf{F}_{\mathrm{d}j}^0$ is negative if dropper j is tensioned. The matrix $\mathbf{K}_\mathrm{dr}$ relates the nodal displacements to the traction force in each dropper, and subscript j extracts the j-th row of a given vector or matrix. If this criterion is not fulfilled for a given dropper, it means it slackens, and an additional correction force must be applied (see more details in [21]). This correction force for the j-th slackened dropper can be computed as:

$$\mathbf{F}_{\mathrm{d}j}^t = \mathbf{F}_{\mathrm{d}j}^0 + \mathbf{I}_{\mathrm{dc}j}F_\mathrm{c}^t + \mathbf{I}_{\mathrm{dd}j}\mathbf{F}_\mathrm{d}^t \tag{4}$$

in which, vector $\mathbf{I}_\mathrm{dc}$ and matrix $\mathbf{I}_\mathrm{dd}$ account for the influence of the contact force and the traction force of each dropper, respectively, on the traction force of each dropper.

2.2. Pantograph and interaction models

A linear lumped-mass model is considered in conventional and real-time numerical simulation (see Section 2.3) to reproduce the dynamic behavior of the ATR 95 pantograph. It consists of three masses, linked with springs and viscous dampers, with vertical degrees of freedom as depicted in Figure 3. If $\mathbf{K}_\mathrm{p}$, $\mathbf{C}_\mathrm{p}$, $\mathbf{M}_\mathrm{p}$ are the stiffness, damping and mass matrices of the pantograph model respectively, and $\mathbf{u}_\mathrm{p}^t = [u_{\mathrm{p}1} \;\; u_{\mathrm{p}2} \;\; u_{\mathrm{p}3}]^\mathrm{T}$ the vector of independent coordinates of the model, the equation of motion of the pantograph can be written as:

$$\mathbf{M}_\mathrm{p}\ddot{\mathbf{u}}_\mathrm{p}^t + \mathbf{C}_\mathrm{p}\dot{\mathbf{u}}_\mathrm{p}^t + \mathbf{K}_\mathrm{p}\mathbf{u}_\mathrm{p}^t = \begin{bmatrix} F_\mathrm{c}^t & 0 & F_{up} \end{bmatrix}^\mathrm{T} \tag{5}$$

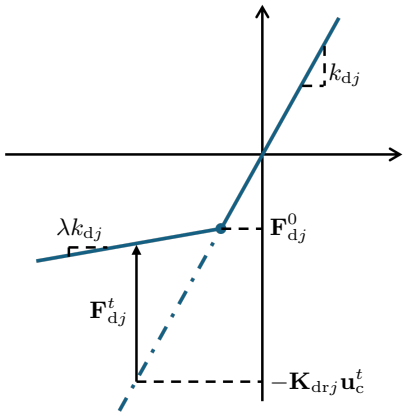


Figure 2: *Bilinear traction-elongation model for a given dropper j. Graphical description of the slackened dropper correction force.*

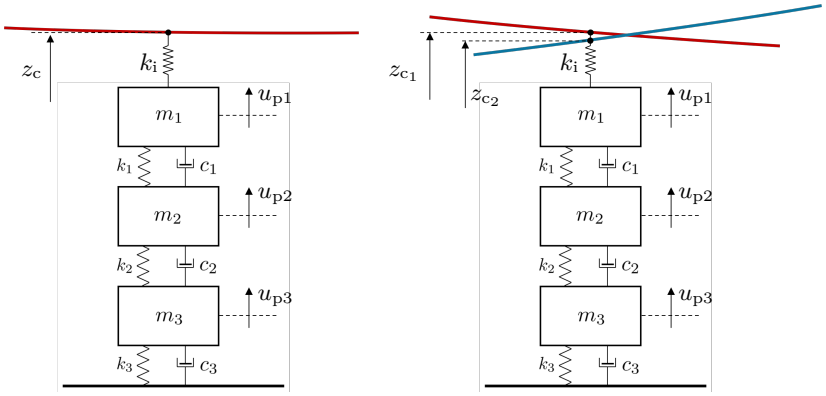


Figure 3: *Lumped-mass pantograph model with a penalty interaction element. Left: Interaction with a single contact wire. Right: simultaneous interaction with two contact wires.*

in which F_{up} is the external uplift force applied to the pantograph model's bottom mass to include the uplift mechanism's load and the aerodynamic force.

The interaction between the pantograph and catenary models is accomplished by introducing a penalty stiffness k_{i} as depicted in Figure 3. The contact force can thus be computed as:

$$F^t_{\mathrm{c}} = \begin{cases} k_{\mathrm{i}}(u^t_{\mathrm{p1}} - z^t_{\mathrm{c}}) & \text{if} \quad u^t_{\mathrm{p1}} > z^t_{\mathrm{c}} \\ 0 & \text{if} \quad u^t_{\mathrm{p1}} \leq z^t_{\mathrm{c}} \end{cases} \tag{6}$$

in which the height of the contact wire at the contact point is:

$$z^t_{\mathrm{c}} = \mathbf{N}^t_{\mathrm{c}} \left(\mathbf{z}^0_{\mathrm{c}} + \mathbf{u}^t_{\mathrm{c}}\right) \tag{7}$$

$\mathbf{z}^0_{\mathrm{c}}$ being the nodal absolute coordinates in the initial configuration of the catenary.

When the pantograph circulates under the overlap section, it can interact simultaneously with the contact wires of each tension length (see Figure 3 right). In this scenario:

$$F_{\mathrm{c}}^{t} = F_{\mathrm{c}_1}^{t} + F_{\mathrm{c}_2}^{t} \tag{8}$$

and Eq. (6) applies to the contact force exerted on each one of the two contact wires, F_{c_1} and F_{c_2}, respectively.

2.3. Conventional vs real-time simulation

To perform a conventional simulation using the models defined in the previous sections with the software PACDIN, the Newmark time integration scheme is applied to solve the coupled Eqs. (2) and (5) for both the catenary and pantograph, respectively, as described in [21]. At each time step, the dropper slackening and contact loss criteria are checked. Given the results of the checking, Eq. (4) is set for every slackened dropper along with Eq. (6). This way, a system of equations is set and solved to obtain both the contact force F_{c}^{t} and the slackened droppers correction forces $\mathbf{F}_{\mathrm{d}}^{t}$. This step is iteratively repeated until the dropper slackening and contact loss criteria outputs do not change in two consecutive iterations.

This conventional simulation algorithm needs some modifications to achieve real-time performance and, therefore, to be applied in a HiL test. First, the contact force is treated explicitly, applying the value computed in the previous time step, F_{c}^{t-1}, to the current contact point. The approximation implied by this simplification is acceptable, provided the time step used in the numerical integration is sufficiently small. Additionally, the catenary model is projected to the modal basis [22]. Eq. (2) thus becomes:

$$\hat{\mathbf{M}}_{\mathrm{c}}\ddot{\mathbf{q}}_{\mathrm{c}}^{t} + \hat{\mathbf{C}}_{\mathrm{c}}\dot{\mathbf{q}}_{\mathrm{c}}^{t} + \hat{\mathbf{K}}_{\mathrm{c}}\mathbf{q}_{\mathrm{c}}^{t} = \hat{\mathbf{N}}_{\mathrm{c}}^{t\mathrm{T}} F_{\mathrm{c}}^{t-1} + \hat{\mathbf{N}}_{\mathrm{d}}^{\mathrm{T}}\mathbf{F}_{\mathrm{d}}^{t} \tag{9}$$

where $(\hat{})$ indicates projection to modal basis and $\mathbf{u}_{\mathrm{c}}^{t} = \Phi\mathbf{q}_{\mathrm{c}}^{t}$, being Φ the modal transformation matrix. With this transformation, after applying the Newmark time integration scheme, the matrix of the resultant system becomes diagonal.

The correction force for the slackened droppers is computed similarly to how it is done in the conventional simulation, i.e. iteratively checking the dropper slackening criterion and solving the system of equations defined in Eq. (4) (including only the equations related to slackened droppers). This system of equations considers the influence that a given correction force has in the internal forces of every dropper. To further reduce computational cost, only a given number of droppers closest to the contact point is checked and corrected if they slacken, thereby reducing the maximum size that this system of equations can have.

Apart from the actions described above, if the real-time performance is not achieved, a coarser finite element mesh and a modal basis truncation can be conducted, provided that the reduction in the accuracy of the results that this entails is within acceptable limits. In summary, the actions taken to transform a conventional pantograph-catenary dynamic interaction simulation to perform a real-time simulation consist of:

A1: Increasing the size of the finite elements in the contact and messenger wires to reduce the number of degrees of freedom of the catenary model.

A2: Treating explicitly the contact force.

A3: Projecting the catenary dynamic model on a N_{mod}-sized truncated modal basis.

A4: Checking only a reduced number of droppers around the contact point to be corrected if they slacken.

3. HiL tests procedure

In a HiL test, the catenary is explicitly treated using Eq.(9), replacing the numerical estimation of the contact force, F_{c}^{t-1}, with the experimentally measured contact force, $F_{\text{c,meas}}^{t-1}$. By solving Eq.(9) the modal solution $\mathbf{q}_{\text{c}}^{t}$ is obtained, which is projected and interpolated using $\hat{\mathbf{N}}_{\text{c}}^{t}$ to obtain the contact wire displacement at the contact point. This is sent as a reference to the vertical actuator that enforces this displacement to the collector head of the pantograph.

As discussed in [14], the previous explicit scheme becomes unstable if the pantograph-catenary interaction occurs through a high stiffness, as that between the contact wire and the contact strip. To avoid this undesirable effect, the use of an interaction mass was proposed in [14], which helps to stabilize the HiL test and to deal with the interaction when there are two contact wires, as in the overlap between two tension lengths. This fictitious system must be designed not to alter the contact force in the 0-20 Hz frequency range, and to have as low an effect as possible above 20 Hz.

3.1. HiL test in the overlap section

Figure 4 schematically represents the contact wires in an overlap between two tension lengths of a catenary. The red line is the outgoing contact wire, which elevates upon the pantograph's passage, while the blue line is the incoming contact wire with a decreasing height. At time t, the interaction mass interacts with both contact wires simultaneously at height $z_{\text{c}}^{t} = z_{\text{c1}}^{t} = z_{\text{c2}}^{t}$ through a stiffness k_{i}. The dynamic behavior of this system is given by Eq.(10), whose solution u_{i}^{t} is the position of the interaction mass loaded with the measured contact force at the previous time step, $F_{\text{c,meas}}^{t-1}$.

$$m_{\text{i}}\ddot{u}_{\text{i}}^{t} + c_{i}\dot{u}_{\text{i}}^{t} + k_{\text{i}}u_{\text{i}}^{t} = k_{\text{i}}z_{\text{c}}^{t} + F_{\text{c,meas}}^{t-1} \tag{10}$$

In this case, u_{i}^{t} is sent as a reference to the vertical actuator. Additionally, it is used to compute the interaction force as:

$$F_{\text{i}}^{t} = k_{\text{i}}\left(u_{\text{i}}^{t} - z_{\text{c}}^{t}\right) \tag{11}$$

The contact wires height, z_{c}^{t}, depends on how the interaction force is distributed among the two wires. To obtain z_{c}^{t} and the forces applied to each wire, F_{i1}^{t} and F_{i2}^{t}, the following three equations are set:

$$\begin{aligned} z_{\text{c}}^{t} &= z_{\text{c1}}^{\text{ini}} + u_{\text{c1}}^{*}F_{\text{i1}}^{t} \\ z_{\text{c}}^{t} &= z_{\text{c2}}^{\text{ini}} + u_{\text{c2}}^{*}F_{\text{i2}}^{t} \\ F_{\text{i1}}^{t} + F_{\text{i2}}^{t} &= F_{\text{i}}^{t-1} \end{aligned} \tag{12}$$

where $z_{\text{c1}}^{\text{ini}}$ and $z_{\text{c2}}^{\text{ini}}$ are the heights of the contact points of the two wires due to the displacement, velocity and acceleration of the catenary at the previous time step. The

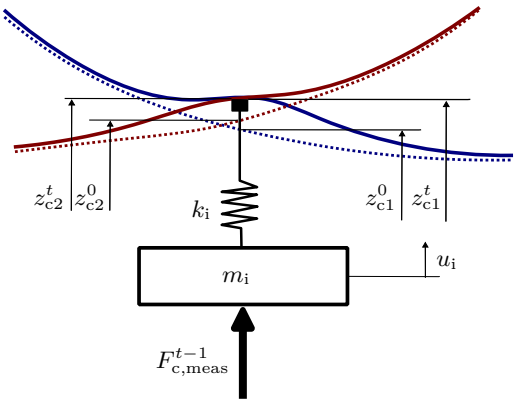


Figure 4: *Interaction mass between the catenary and the pantograph models.*

coefficients u^*_{c1} and u^*_{c2} are the displacements of the contact points of the two wires after a time step caused by a unitary vertical force applied to the contact wires 1 and 2, respectively, and are precomputed previously to the HiL test (see [21, 22] for more details).

It is important to note that the interaction force used is that from the previous time step, F_i^{t-1}. This implies that the problem is solved as if the interaction mass were part of the pantograph and the dynamic problem is addressed explicitly.

Thus, a new action on the models to move from a conventional simulation to a HiL test must be added to the list provided in Section 2.3. That is:

A5: Adding an interaction mass to stabilize the HiL test.

3.2. LQG controller

The principle of the HiL testing method is shown in Figure 5. By solving Eq. (12), z_c^t is obtained, which, along with the interaction force measured at the previous time step, $F^{t-1}_{c,meas}$, allows computing the new position of the interaction mass, u_i, according to Eq. (10), which is sent as a reference to the vertical actuator. This linear motor moves the pantograph collector head, producing a contact force.

In addition to vertical displacement, the test rig allows for lateral motion to simulate the contact wire stagger through a horizontal actuator. Regarding lateral movement, only the static position of the catenary is considered; thus, the reference is not adjusted to account for dynamic catenary deformation. This predefined lateral trajectory is shown in Figure 6. Within the overlap zone, the reference is calculated as a weighted average of the lateral positions of both contact wires, ensuring a smooth transition from one tension length to the next. Finally, the reference signal sent to the horizontal motor is processed using a 6th-order low-pass filter with a 5 Hz cut-off frequency.

In this setup, two communication delays are observed due to: i) transmission of u_i as a reference to the linear actuator and ii) measurement of the contact force.

These delays, if not properly managed, may lead to unstable behavior of the HiL test. To avoid that, the use of an LQG controller is proposed (see [14] for more details). This controller modifies the reference signal u_i by adding the term u_{lqg}. Since LQG is

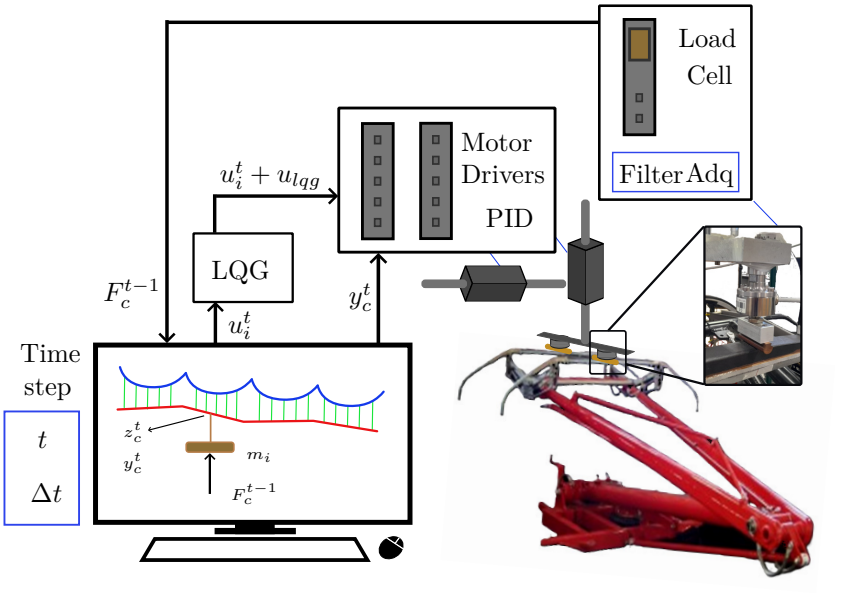


Figure 5: *Scheme of the Hardware-in-the-Loop components and workflow.*

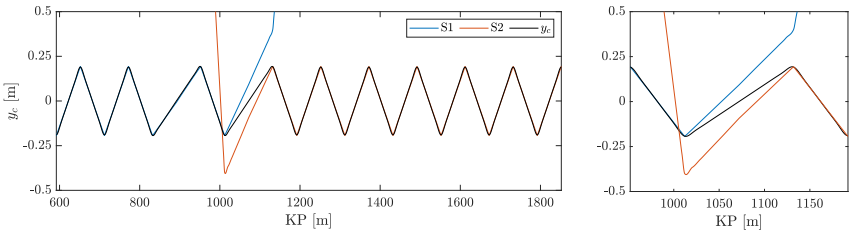


Figure 6: *Static equilibrium lateral position of the contact wire for tension lengths S1 (blue line) and S2 (orange line), including the reference signal sent to the lateral actuator (black line). The right plot shows an enlarged view of the overlap section.*

a full-state feedback control scheme, it requires an estimate of the dynamic models of both the pantograph and the linear actuator, as well as knowledge of the actual contact stiffness between the actuator and the contact strips, k_p.

The controller is designed using a simplified model of the HiL components, as shown in the block diagram of Figure 7, where u_m and u_p denote the positions of the actuator and of the pantograph, respectively. The controller aims to minimize the difference between the reference displacement sent to the actuator (represented in Figure 7 by block G_m), u_i, and its actual position, u_m. The contact point position, z_c, is considered as a disturbance of the system. In the simplified model, both the linear actuator and the pantograph are modeled as second-order systems, each one defined by three parameters (m, c, and k),

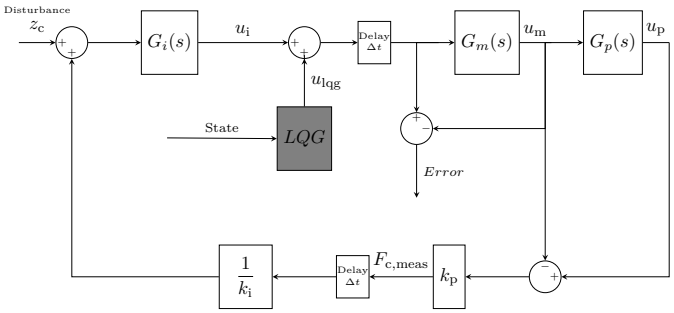


Figure 7: *Block diagram of the LQG controller.*

whose Laplace-domain representation is:

$$G_{\mathrm{m}}(s) = \frac{k_{\mathrm{m}}}{m_{\mathrm{m}}\, s^2 + c_{\mathrm{m}}\, s + k_{\mathrm{m}}} \qquad G_{\mathrm{p}}(s) = \frac{k_{\mathrm{p}}}{m_{\mathrm{p}}\, s^2 + c_{\mathrm{p}}\, s + k_{\mathrm{p}}} \tag{13}$$

The complete simplified model includes therefore 8 states, 6 from the three dynamic systems (position and velocity of the linear actuator, the pantograph, and the interaction mass), and 2 due to the delays in the system. Thus, the corrective action of the linear actuator can be computed as:

$$u_{\mathrm{lqg}} = \mathbf{K}_{\mathrm{lqg}}\, \mathbf{x}_0 \tag{14}$$

where $\mathbf{x}_0$ is the state vector and $\mathbf{K}_{\mathrm{lqg}}$ is the 1×8 controller matrix, which is constant assuming a linear model.

The parameters of the models used to obtain the controller matrix are listed in Table 1. This controller is derived from a disturbance rejection control problem, in which the difference between the displacement of the interaction mass and the linear actuator, $u_{\mathrm{i}} - u_{\mathrm{m}}$, is minimized for any disturbance z_{c} of the system, while keeping the corrective action u_{lqg} as low as possible. Thus, the optimization problem to be solved is:

$$\min_{u_{\mathrm{lqg}}} \sum_{t=1}^{\infty} Q\,(u_{\mathrm{i}} - u_{\mathrm{m}})^2 + R\,(u_{\mathrm{lqg}})^2 \tag{15}$$

in which the relative weight of the two terms is defined by the two scalar coefficients Q and R. The state observer is a Kalman filter that uses the measurements of the linear actuator and the interaction mass positions, with a process noise covariance R_{kf} and a measurement noise covariance Q_{kf}. These parameters are also shown in Table 1.

	m (kg)	c (N/ms)	k (N/m)
Mass	0.1	10	50.000
Motor	10	1.800	450.000
Pantograph	9.3	10	350.000

R	Q	R_{kf}	Q_{kf}
1	5	10^{-3}	10

Table 1: *Parameters used for the design of the LQG controller.*

4. Results and validation

4.1. Validation of the real-time catenary model

This section aims to validate the real-time catenary model and solver used in the HiL tests. For that purpose, the same pantograph-catenary dynamic interaction problem is solved by both the conventional and real-time algorithms. The catenary, pantograph and interaction models are those described in Section 2.1. The time step used is $\Delta t = 2$ ms and the train running speed is $v = 301.5$ km/h. With this setup, the pantograph takes 20.06 s from position 172 m to 1852 m. The simulation begins with the pantograph gradually making contact with the wire, followed by an initial travel over several spans to avoid transient effects due to initialization. This segment is graphically indicated by a dashed gray band in Figure 1. Consequently, the analysis section covers the track from position 592 m to 1852 m, also highlighted in Figure 1 with a solid gray band. The stiffness of the slackened droppers is considered null ($\lambda = 0$), while the penalty stiffness of the interaction model is set to $k_\mathrm{i} = 50000$ N/m.

Recalling that the differences between the conventional and real-time solvers are due to modifications according to the four actions listed in Section 2.3 and action A5 described in Section 3.1, Table 2 summarizes the main features of both models (the tension lengths of the catenary, S1 and S2 respectively, as denoted in Figure 1) and solvers according to each action. In this specific case, A1 consisted of reducing to almost half the degrees of freedom of each of the two tension lengths by increasing the length of the beam elements used to model both the contact and messenger wires. A2 implies that the contact force F_c^t is treated explicitly, and computed from the pantograph model in this numerical scenario. While the conventional model is formulated in physical coordinates, in the real-time model, after taking A3 and applying the procedure proposed in [22], a truncated modal base of 8000 modes for each tension length is considered. In the conventional solver, the dropper correction criterion (see Eq. (3)) is applied to the 147 and 166 droppers of the tension lengths 1 and 2, respectively. However, in the real-time solver, only the 8 droppers closest to the contact point are checked for slackening correction. Finally, to assess the effect of action A5, the interaction mass is linked to the catenary model to stabilize the system when used in a HiL test.

Table 2: *Main features of the conventional and real-time model and solver regarding the five simplifying actions to move from the former to the latter.*

	Conventional		**Real-time**	
	S1	S2	S1	S2
A1	20256 d.o.f.	22774 d.o.f.	10356 d.o.f.	11614 d.o.f.
A2	Panto. model mandatory		Panto. model mandatory	
A3	Physic coordinates		8000 modes	8000 modes
A4	147 droppers	166 droppers	8 droppers	
A5	Without interaction mass		With interaction mass	

The 20 Hz filtered contact force obtained from both solvers is shown in Figure 8. Looking at this figure, we can confirm that the actions taken to move from the conventional algorithm to the real-time algorithm have not significantly modified the results

obtained. Additionally, Figure 8 includes an enlarged view of the overlap section, where the contact transition from one tension length to the other occurs.

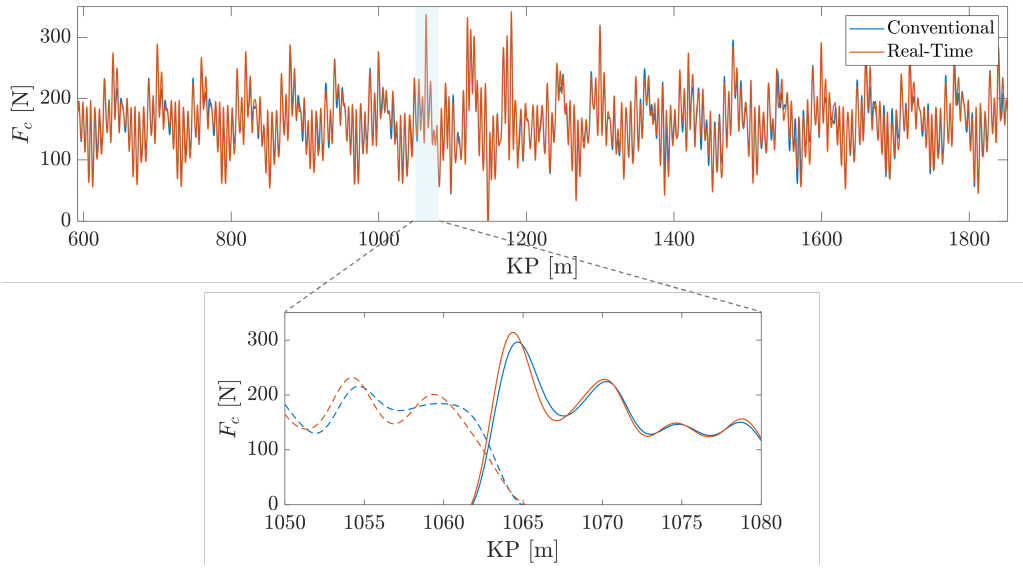


Figure 8: *Comparison of the 20 Hz filtered contact force obtained from the conventional and real-time solver. Includes an enlarged view of the overlap section, separately depicting the contact forces for S1 (dashed line) and S2 (solid line).*

To quantify the differences between these two results, the relative root mean squared error between the contact force obtained from the conventional model, $\mathbf{F}_{\mathrm{c}_{\mathrm{conv}}}$, and that obtained from the real-time model, $\mathbf{F}_{\mathrm{c}_{\mathrm{RT}}}$, is defined as:

$$\mathrm{RRMSE} = \frac{\|\mathbf{F}_{\mathrm{c}_{\mathrm{conv}}} - \mathbf{F}_{\mathrm{c}_{\mathrm{RT}}}\|}{\|\mathbf{F}_{\mathrm{c}_{\mathrm{conv}}}\|} \tag{16}$$

where the operator $\|\cdot\|$ is the Euclidean norm. The plot on the left of Figure 9 shows this error indicator for the contact force obtained after applying each one of the five simplifying actions cumulatively, i.e., A4 stands for the contact force obtained with a solver that includes from A1 to A4. It can be seen that after coarsening the finite element mesh and treating the interaction force explicitly, the RRMSE with respect to the conventional simulation results reaches approximately 7.5 %. After that, the projection to a truncated modal basis slightly increases the error in the obtained interaction force because the number of modes considered is high enough compared to the total degrees of freedom of the catenary model. A further small increase is observed due to the constraint of accounting for slackening correction only for the eight droppers closest to the contact point in each time step. Finally, the introduction of the interaction mass does not significantly alter the error, which in this case is slightly reduced. This RRMSE value slightly increases to 8.3 % for the three spans nearest to the overlap section (from 1012 m to 1192 m), which confirms the validity of the real-time algorithm even within the singular region of the overlap.

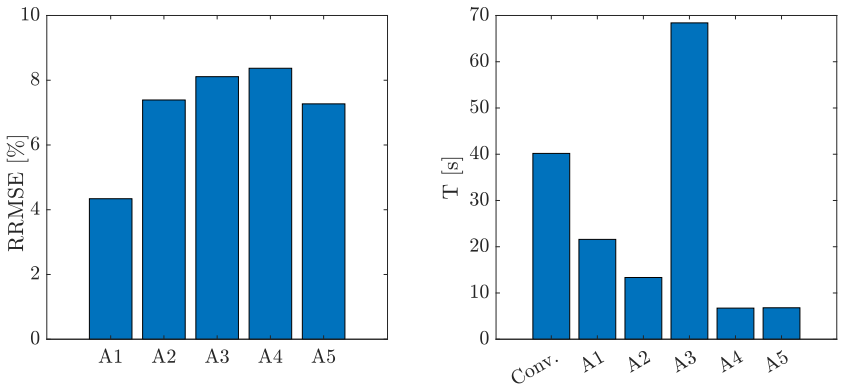


Figure 9: *Effect of taking the five simplifying actions on the conventional model and solver. Left plot: Relative root mean square error of the contact force. Right plot: Computational time to solve the dynamic interaction problem.*

On the other hand, the right plot of Figure 9 depicts the computational cost required to solve the dynamic interaction problem itself without considering the computational cost of pre-computing some required matrices and vectors. The simulations were run on an Intel® i9-12900KF processor with 128 GB RAM. In this case, every action taken on the catenary model or solver reduces the time consumed to obtain the solution, except for Action 3, which consists of projecting the catenary dynamics on a truncated modal basis. This occurs because the application of the slackening criterion in modal coordinates (the projection of Eq. (3) to the modal basis) requires performing the product of the $N_{\mathrm{dr}} \times N_{\mathrm{mod}}$ matrix $\hat{\mathbf{K}}_{\mathrm{dr}}$ with the $N_{\mathrm{mod}} \times 1$ vector $\mathbf{q}_{\mathrm{c}}^{t}$, which is computationally more demanding. However, A3 enables A4 to be executed, and the size of matrix $\hat{\mathbf{K}}_{\mathrm{dr}}$ becomes $8 \times N_{\mathrm{mod}}$, which leads to a relevant decrease in the computational cost from almost 70 s to only 6.7 s. As can be seen, the introduction of the interaction mass does not modify the computational cost of the simulation.

4.2. Comparison of HiL results with in-line measurements

In this section, the results obtained from a Hardware-in-the-Loop (HiL) test are validated against in-line measurements performed with a pantograph instrumented and calibrated according to EN50317 [2]. The in-line measurements were acquired with a sampling frequency of 100 Hz, while the HiL test was conducted with a time step of 2 ms. To ensure a proper comparison, the contact force obtained from the HiL test is resampled at the same kilometric points at which the in-line measurements were taken. In the HiL test, the stiffness of the droppers in compression was set to 0.5 % of their tensile stiffness ($\lambda = 0.005$), reflecting realistic dropper slackening effects.

The 20 Hz low-pass filtered contact force, along with its frequency spectrum, is compared for the in-line measurements and the HiL test in Figure 10, following the assessment criteria established for current collection quality. The general trend observed in the contact force is very similar in both cases, displaying a repetitive pattern due to span passage. This pattern is interrupted around KP = 1072 m as the pantograph passes under the overlap section, which represents a significant geometric singularity. The standard devi-

ation of the in-line measurement is 48.6 N, while that of the HiL result is 51.6 N. This leads to a relative difference of 6.2 %, which is well below the 20 % accuracy threshold required by the EN 50318 standard [23]. Within the overlap section (from 1012 m to 1192 m), the relative difference increases to 13.9 %, yet remains within the acceptable limits defined in [23].

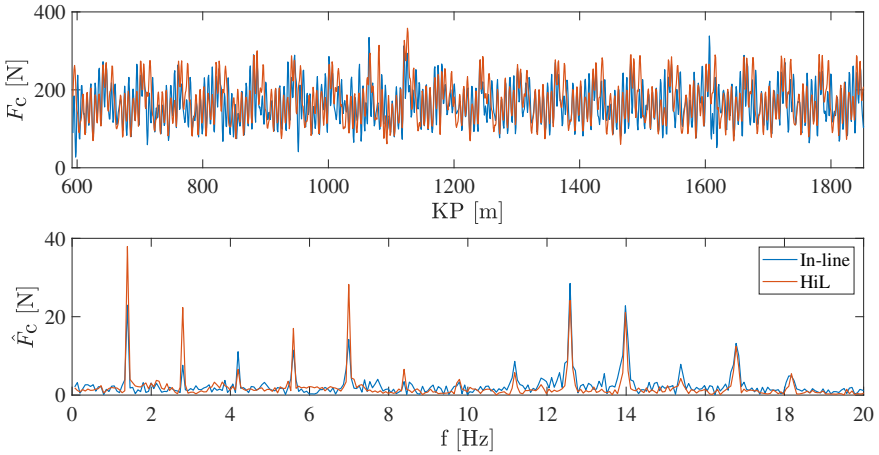


Figure 10: *Time domain (above) and spectrum (bottom) comparison of the 20 Hz filtered contact force obtained from in-line measurements and HiL tests.*

Upon analyzing the spectrum, the primary frequency content is centered at the harmonics of the span passing frequency, which corresponds to 1.4 Hz for a vehicle speed of 301.5 km/h. The agreement between the HiL test results and in-line measurements is high for frequencies exceeding 8 Hz, a range where the influence of nonlinear dropper behavior becomes evident. Specifically, the selection of $\lambda = 0.005$ for compressive stiffness facilitates this close matching in the high-frequency band.

However, below 8 Hz, the frequency content of the contact force resulting from the HiL test is notably higher than that of the in-line measurement. A probable cause for this discrepancy is that the HiL test utilized a catenary model based on nominal design data. In contrast, the actually installed catenary, where in-line measurements were acquired, likely exhibits uneven contact wire height due to manufacturing and installation errors, wear, and other geometric irregularities. Numerical tests previously conducted by the authors indicate that contact wire height irregularities exert a significant influence on the lower frequency band of the contact force, which further supports this hypothesis as the source of the observed differences.

5. Conclusions

This paper presented a comprehensive methodology for high-fidelity Hardware-in-the-Loop (HiL) tests, bridging the gap between numerical models and experimental field testing. By utilizing realistic catenary models, this research provides a lab-based alternative to line tests that meets the stringent railway certification accuracy requirements.

A high-fidelity model of the Italian C270 catenary was successfully developed, explicitly incorporating complex features such as overlap sections. The simultaneous interaction of the ATR 95 pantograph with two contact wires in the overlap was addressed through a specific penalty-based contact formulation and the use of an interaction mass to ensure system stability. Furthermore, the inclusion of a realistic dropper model that accounts for compressive stiffness proved essential for capturing the high-frequency dynamics of the contact force.

A significant contribution of this work is the adaptation of the PACDIN conventional solver into a real-time algorithm through five simplifying hypotheses. These actions reduced the computational cost by approximately six times (from 40 s to 6.7 s) while maintaining a high accuracy. Furthermore, the implementation of an LQG controller for precise force tracking substantially improved the stability and accuracy of HiL tests.

The methodology was validated in a two-stage process, first confirming that the real-time algorithm maintains excellent agreement with the high-fidelity conventional numerical solver. Subsequently, the HiL test results were compared against experimental in-line measurements obtained with an instrumented pantograph. The standard deviation of the contact force showed a relative difference of only 6.2 %, which falls within the acceptable limits for the validation of pantograph-catenary interaction simulation tools [23]. Although some discrepancies were observed at lower frequencies due to nominal data assumptions, the satisfactory overall matching confirms that this HiL environment is a robust tool for studying complex pantograph-catenary interaction phenomena.

This research represents a significant milestone toward the potential replacement of expensive line tests with high-precision laboratory tests. To further advance this transition, future work will focus on enhancing the fidelity of the test bench by incorporating independent actuation for each collector strip. Additionally, the methodology will be expanded to account for full carbody dynamics. Finally, the robustness of the framework needs to be validated across a broader range of infrastructures, such as double-contact wire systems and rigid overhead conductor rails, to facilitate its adoption as a standardized industrial certification tool.

Funding details

Grant PID2023-148854OB-C21 funded by MICIU/AEI/10.13039/501100011033 and by "ERDF/EU".

Disclosure statement

The authors report there are no competing interests to declare.

Data availability

The data that support the findings of this study are available from the corresponding author, S. Gregori, upon reasonable request.

Appendix A. Geometric and material input parameters

The catenary modeled in this work corresponds to the Italian C270 high-speed catenary. This model consists of two tension lengths of the overhead contact line of the line Torino-Milano, which spans from kilometer 54.485 to 56.757, corresponding to a total length of the model of 2272 m, as shown in Figure 1. Table A.1 details the geometric definition of the first tension length, including the staggered position of the contact wire at each mast, the heights of the contact and messenger wires, and the number of droppers per span. The geometry of the second tension length is provided in A.2.

Table A.1: *Geometry definition of the first tension length.*

Mast	Span	Span Length (m)	Stagger (m)	CW Height (m)	MW Height (m)	Droppers
1	-	-	-2.0	6.800	7.00	-
2	1	58	0.4	5.800	6.70	-
3	2	58	0.1	5.333	6.70	3
4	3	56	-0.2	5.300	6.70	7
5	4	60	0.2	5.300	6.55	9
6	5	60	-0.2	5.300	6.55	9
7	6	60	0.2	5.300	6.55	9
8	7	60	-0.2	5.300	6.55	9
9	8	60	0.2	5.300	6.55	9
10	9	60	-0.2	5.300	6.55	9
11	10	60	0.2	5.300	6.55	9
12	11	60	-0.2	5.300	6.55	9
13	12	60	0.2	5.300	6.55	9
14	13	59	-0.2	5.300	6.55	9
15	14	59	0.2	5.300	6.55	9
16	15	59	0.0	5.300	6.55	9
17	16	59	-0.2	5.300	6.55	9
18	17	59	0.2	5.300	6.70	9
19	18	59	-0.1	5.333	6.70	8
20	19	60	-0.4	5.800	6.70	3
21	20	60	-2.0	6.800	7.00	-

Table A.2: *Geometry definition of the second tension length.*

Mast	Span	Span Length (m)	Stagger (m)	CW Height (m)	MW Height (m)	Droppers
1	-	-	-2.0	6.800	7.00	-
2	1	60	0.4	5.800	6.70	-
3	2	60	0.1	5.333	6.70	3
4	3	60	-0.2	5.300	6.70	8
5	4	60	0.2	5.300	6.55	9
6	5	60	-0.2	5.300	6.55	9
7	6	60	0.2	5.300	6.55	9
8	7	60	-0.2	5.300	6.55	9
9	8	60	0.2	5.300	6.55	9
10	9	60	-0.2	5.300	6.55	9
11	10	60	0.2	5.300	6.55	9
12	11	60	-0.2	5.300	6.55	9
13	12	60	0.2	5.300	6.55	9
14	13	60	-0.2	5.300	6.55	9
15	14	60	0.2	5.300	6.55	9
16	15	60	-0.2	5.300	6.55	9
17	16	60	0.2	5.300	6.55	9
18	17	60	0.0	5.300	6.55	9
19	18	60	-0.2	5.300	6.55	9
20	19	60	0.2	5.300	6.70	9
21	20	60	-0.1	5.333	6.70	8
22	21	60	-0.4	5.800	6.70	3
23	22	60	-2.0	6.800	7.00	-

Table A.3 reports the Young's modulus, cross-section, and material density for the messenger wire, contact wire, and droppers. For the first two components, which are modeled using ANCF beam elements, the second moment of area is also defined. Additionally, the mechanical tension applied to both cables by the compensation system (counterweights and pulleys) is listed. For the steady arms, Table A.3 also lists their mass and length.

Table A.3: *Material properties and parameters of the different catenary components.*

Component	E (GPa)	A (m^2)	ρ (kg/m^3)	I (m^4)	T (kN)	m (kg)	L (m)
Messenger wire	120	$1.2 \cdot 10^{-4}$	8925	$1.0975 \cdot 10^{-9}$	16.25	-	-
Contact wire	120	$1.5 \cdot 10^{-4}$	8890	$1.625 \cdot 10^{-9}$	20.00	-	-
Droppers	85	$1.2 \cdot 10^{-5}$	9307	-	-	-	-
Steady arms	7.0	$2.7037 \cdot 10^{-4}$	2700	-	-	0.8	1.2165

Finally, Table A.4 specifies the masses of the different types of clamps used to connect the various elements of the overhead contact line. Specifically, the masses for the messenger wire-dropper clamp, the contact wire-dropper clamp, and the steady arm-contact

wire clamp are provided.

Table A.4: *Mass of the clamps used for the connection between different catenary components.*

Component	Mass (kg)
Messenger wire - Dropper clamp	0.195
Contact wire - Dropper clamp	0.165
Steady arm - Contact wire clamp	0.150

In addition to the aforementioned data, the model incorporates a vertical stiffness of 455 kN/m at the messenger wire supports and utilizes a proportional Rayleigh damping model defined by the constants $\alpha = 0.0125$ s^{-1} and $\beta = 10^{-4}$ s.

References

[1] F. Kiessling, R. Puschmann, A. Schmieder, E. Schneider, Contact lines for electric railways: planning, design, implementation, maintenance, John Wiley & Sons, 2018.

[2] EN 50317:2025, Railway applications. Current collection systems. Requirements for and validation of measurements of the dynamic interaction between pantograph and overhead contact line, *European Committee for Electrotechnical Standardization (CENELEC)* (2025).

[3] EN 50367:2022, Railway applications. Fixed installations and rolling stock. Criteria to achieve technical compatibility between pantographs and overhead contact line, *European Committee for Electrotechnical Standardization (CENELEC)* (2012).

[4] S. Bruni, G. Bucca, A. Facchinetti, S. Gregori, J. Pombo, Recent developments on pantograph-overhead line interaction, Vehicle System Dynamics 63 (7) (2025) 1358–1394.

[5] W. Zhang, G. Mei, X. Wu, Z. Shen, Hybrid simulation of dynamics for the pantograph-catenary system, *Veh. Syst. Dyn.* 38 (6) (2002) 393–414. doi:10.1076/vesd.38.6.393.8347.

[6] W. Zhang, G. Mei, X. Wu, L. Chen, A study on dynamic behaviour of pantographs by using hybrid simulation method, *Proc. Inst. Mech. Eng. F: J. Rail Rapid Transit* 219 (3) (2005) 189–199. doi:10.1243/095440905X8880.

[7] F. Resta, A. Facchinetti, A. Collina, G. Bucca, On the use of a hardware in the loop set-up for pantograph dynamics evaluation, *Veh. Syst. Dyn,* 46 (S1) (2008) 1039–1052. doi:10.1080/00423110802037891.

[8] A. Correcher, C. Ricolfe-Viala, M. Tur, S. Gregori, M. Salvador-Muñoz, F. J. Fuenmayor, J. Gil, A. M. Pedrosa, Hardware-in-the-loop test bench for simulation of catenary–pantograph interaction (cpi) with linear camera measurement, Sensors 23 (4) (2023) 1773.

[9] A. Facchinetti, S. Bruni, Hardware-in-the-loop hybrid simulation of pantograph–catenary interaction, Journal of Sound and Vibration 331 (12) (2012) 2783–2797.

[10] A. Facchinetti, L. Gasparetto, S. Bruni, Real-time catenary models for the hardware-in-the-loop simulation of the pantograph–catenary interaction, Vehicle System Dynamics 51 (4) (2013) 499–516. arXiv:https://doi.org/10.1080/00423114.2012.748920, doi:10.1080/00423114.2012.748920. URL https://doi.org/10.1080/00423114.2012.748920

[11] J. Gil, M. Tur, A. Correcher, S. Gregori, A. Pedrosa, F. Fuenmayor, Hardware-in-the-loop pantograph tests using analytical catenary models, Vehicle System Dynamics 60 (10) (2022) 3504–3518.

[12] D. Ritzberger, E. Talic, A. Schirrer, Efficient simulation of railway pantograph/catenary interaction using pantograph-fixed coordinates, IFAC-PapersOnLine 48 (1) (2015) 61–66.

[13] J. Gil, M. Tur, S. Gregori, A. Correcher, A. M. Pedrosa, F. Fuenmayor, Hardware-in-the-loop simulations of a railway pantograph with a finite element periodic catenary model, Vehicle System Dynamics 62 (3) (2024) 695–718.

[14] A. C. J. G. A. M. P. F. J. F. M. Tur, S. Gregori, Hardware-in-the-loop pantograph tests with general overhead contact line geometry, Mechatronics 102 (2024) 103231.

[15] A. Schirrer, G. Aschauer, E. Talic, M. Kozek, S. Jakubek, Catenary emulation for hardware-in-the-loop pantograph testing with a model predictive energy-conserving control algorithm, Mechatronics 41 (2017) 17 – 28.

[16] S. KOBAYASHI, Y. YAMASHITA, T. USUDA, D. P. STOTEN, Hybrid simulation testing of a pantograph-catenary system using a dynamically substructured system framework and a mdof catenary model, Quarterly Report of RTRI 61 (2) (2020) 127–132.

[17] L. Calvanese, A. Facchinetti, et al., A new methodology for hybrid simulation of pantograph-catenary interaction based on hybrid system response convergence: Proposal and first numerical and experimental tests, in: Civil-Comp Conferences, Vol. 7, Civil-Comp Press, 2024, pp. 1–14.

[18] M. Tur, L. Baeza, F. Fuenmayor, E. García, Pacdin statement of methods, Vehicle System Dynamics 53 (3) (2015) 402–411.

[19] M. Berzeri, A. Shabana, Development of simple models for the elastic forces in the absolute nodal co-ordinate formulation, Journal of Sound and Vibration 235 (4) (2000) 539–565. doi:10.1006/jsvi.1999.2935.

[20] M. Tur, E. García, L. Baeza, F. Fuenmayor, A 3D absolute nodal coordinate finite element model to compute the initial configuration of a railway catenary, Engineering Structures 71 (2014) 234–243. doi:10.1016/j.engstruct.2014.04.015.

[21] S. Gregori, M. Tur, E. Nadal, J. V. Aguado, F. J. Fuenmayor, F. Chinesta, Fast simulation of the pantograph–catenary dynamic interaction, *Finite Elem. Anal. Des.* 129 (2017) 1 – 13. doi:10.1016/j.finel.2017.01.007.

[22] S. Gregori, M. Tur, A. Pedrosa, J. Tarancón, F. Fuenmayor, A modal coordinate catenary model

for the real-time simulation of the pantograph-catenary dynamic interaction, *Finite Elem. Anal. Des.* 162 (2019) 1–12. doi:10.1016/j.finel.2019.05.001.

[23] EN 50318:2018, Railway applications. Current collection systems. Validation of simulation of the dynamic interaction between pantograph and overhead contact line, *European Committee for Electrotechnical Standardization* (2018).